

Broadband multi-channel quantum noise suppression and phase-sensitive modulation based on entangled beam

Ke Di(邸克), Shuai Tan(谈帅), Anyu Cheng(程安宇), Yu Liu(刘宇), and Jiajia Du(杜佳佳)
Citation: Chin. Phys. B, 2023, 32 (**10**): 100302. DOI: 10.1088/1674-1056/acd8a8
Journal homepage: http://cpb.iphy.ac.cn; http://iopscience.iop.org/cpb

What follows is a list of articles you may be interested in

Effects of quantum quench on entanglement dynamics in antiferromagnetic Ising model

Yue Li(李玥), Panpan Fang(房盼盼), Zhe Wang(王哲), Panpan Zhang(张盼盼), Yuliang Xu(徐玉良), and Xiangmu Kong(孔祥木)
Chin. Phys. B, 2023, 32 (**10**): 100303. DOI: 10.1088/1674-1056/ace15c

Entanglement properties of superconducting qubits coupled to a semi-infinite transmission line

Yang-Qing Guo(郭羊青), Ping-Xing Chen(陈平形), and Jian Li(李剑)
Chin. Phys. B, 2023, 32 (**6**): 060302. DOI: 10.1088/1674-1056/acc0fa

Generation of microwave photon perfect *W* states of three coupled superconducting resonators

Xin-Ke Li(李新克), Yuan Zhou(周原), Guang-Hui Wang(王光辉), Dong-Yan Lv(吕东燕),Fazal Badshah, and Hai-Ming Huang(黄海铭)
Chin. Phys. B, 2023, 32 (**4**): 040306. DOI: 10.1088/1674-1056/aca394

Characterizing entanglement in non-Hermitian chaotic systems via out-of-time ordered correlators

Kai-Qian Huang(黄恺芊), Wei-Lin Li(李蔚琳), Wen-Lei Zhao(赵文垒), and Zhi Li(李志)
Chin. Phys. B, 2022, 31 (**9**): 090301. DOI: 10.1088/1674-1056/ac67c3

Effects of colored noise on the dynamics of quantum entanglement of a one-parameter qubit—qutrit system

Odette Melachio Tiokang, Fridolin Nya Tchangnwa, Jaures Diffo Tchinda,Arthur Tsamouo Tsokeng, and Martin Tchoffo
Chin. Phys. B, 2022, 31 (**5**): 050306. DOI: 10.1088/1674-1056/ac2f36

Broadband multi-channel quantum noise suppression and phase-sensitive modulation based on entangled beam

Ke Di(邸克), Shuai Tan(谈帅), Anyu Cheng(程安宇), Yu Liu(刘宇), and Jiajia Du(杜佳佳)†

Chongqing University of Post and Telecommunications, Chongqing 400065, *China*

(Received 2 February 2023; revised manuscript received 19 May 2023; accepted manuscript online 25 May 2023)

We present a theoretical scheme for broadband multi-channel quantum noise suppression and phase-sensitive modulation of continuous variables in a coupled resonant system with quantum entanglement properties. The effects of different coupling strengths, pumping power in suppressing quantum noise and controlling the width of quantum interference channels are analyzed carefully. Furthermore, quantum noise suppression at quadrature amplitude is obtained with phase-sensitive modulation. It shows that the entanglement strength of the output field and the quantum noise suppression effect can be enhanced significantly by a strong pumping filed due to interaction of pumping light with the nonlinear crystal. The full width at half maxima (FWHM) of the noise curve at the resonant peak ($\Delta = 0$ MHz) is broadened up to 2.17 times compared to the single cavity. In the strong coupling resonant system, the FWHM at $\Delta = 0$ MHz ($\Delta = \pm 3.1$ MHz) is also broadened up to 1.27 (3.53) times compared to the weak coupling resonant system case. The multi-channel quantum interference creates an electromagnetically induced transparent-like line shape, which can be used to improve the transmission efficiency and stability of wave packets in quantum information processing and quantum memory.

Keywords: quantum entanglement, broadband quantum interference, phase-sensitive modulation

PACS: 03.65.Ud, 42.50.Lc, 42.65.Yj **DOI:** 10.1088/1674-1056/acd8a8

1. Introduction

Entangled state optical fields are widely studied since they are an essential resource in next-generation quantum communication technologies. They have been applied in quantum secret key distribution,[1,2] quantum secret key sharing,[3,4] quantum teleportation.[5,6] An entangled state light field can exist in both discrete variable and continuous variable forms. Discrete variables of entangled photon pair have excellent fidelity.[7,8] However, an entangled light field in continuous variable has many advantageous such as superior broadband, excellent stabilization, and high operating efficiency.[9,10] The continuous variable of quantum entangled beam at 1550 nm communication band wavelength was produced by Feng *et al.*[11] Wen *et al.* proposed a scheme for tunable three-mode entanglement of continuous variable.[12] Two-mode entangled-state beams are applied within miniature waveguide circuits, which is a crucial step towards fully integrated quantum information.[13] The transmission threshold of quantum repeater can be enhanced by manipulating a continuous variable entangled state of optical fields.[14]

Entangled light has important applications in the field of quantum communication. Considering the decay of light beams during propagation, it has been introduced into optical parametric amplification systems to study relevant properties. Ma *et al.* investigated mode splitting within the transmission spectrum of a phase-sensitive optical parametric amplifier in a single optical parametric amplifier (OPA) system.[15] Reflected field quantum fluctuation interference was demonstrated theoretically in a single OPA system by Agarwal.[16] Later, Chen *et al.* applied entangled light to a single OPA system and produced electromagnetically induced transparent-like (EIT-like) line shape phenomena at the $\Delta = 0$ MHz.[17] All of the above studies were in single OPA systems. The scheme of Chen *et al.* is more similar to ours. However, their scheme only produces quantum coherence effects at $\Delta = 0$ MHz and has a narrow window for such coherence effects. Our scheme is achieved in a coupled resonant cavity system. It turns out that quantum noise suppression windows can be generated at multiple detuning frequencies. As the coupling strength of the model is increased, the width of the quantum noise suppression windows can be significantly broadened. Di *et al.* experimentally achieved induced transparency in coupled resonant systems.[18] However, a squeezed field was injected into their system without nonlinear crystal. Hence the parametric down-conversion cannot occur. As the results in this study, it can be seen that nonlinear crystals play an important role in broadening the quantum noise suppression windows.

In this paper, we provide a multi-channel quantum entanglement scheme in a coupling resonant system which consists of a periodically poled potassium titanyl phosphate (PPKTP) crystal and two cavities. The PPKTP crystal is driven by pumping light and embedded in cavity C_2. We carefully investigate the multi-channel quantum interference and entanglement properties of the system with phase-sensitive modulation. A detailed comparison between the OPA resonant cavity and the coupling resonant cavity is also presented. Our results show that the coupling resonant system generates the entanglement properties of multi-channel simultaneously, and the

†Corresponding author. E-mail: dujj@cqupt.edu.cn

© 2023 Chinese Physical Society and IOP Publishing Ltd

strong coupling resonant cavity can broaden the bandwidth of each channel by 2–3.5 times. The nonlinear crystal enhances the entanglement strength of the output field as the entangled light is injected into the system. Furthermore, quantum noise suppression at quadrature amplitude is achieved with phase-sensitive modulation, which can be applied to improve measurement accuracy. Each broadband quantum interference channel presents an EIT-like line shape, which is expected to be applied in quantum information processing[19] and quantum memory to improve the transmission stability of wave packet.[20–22]

2. Theoretical model

Figure 1 schematically shows a coupling resonant system. The coupling resonant cavity consists of two flat-concave mirrors M_{front}, M_{bac}, and a plane mirror M_{mid}. Cavities C_1 and C_2 are connected by a plane mirror M_{mid}. The coupling coefficient depends on the reflectivity rate of the middle cavity mirror. A nonlinear crystal is placed at the center of cavity C_2. Cavity C_2 in Fig. 1(a) consists of a flat-concave mirror M_{bac}, a plane mirror M_{mid}, and a nonlinear crystal (PPKTP), which form an OPA system. The threshold limit is defined as $\beta_{th} = (\gamma_p\sqrt{\gamma_1\gamma_2})/g$. Here β is the amplitude of the pumping light, and g is the nonlinear susceptibility. The function of the scaled pumping amplitude is defined as $E_{th} = \frac{|\beta|}{|\beta_{th}|}$.[23] The OPA system we studied works $E_{th} < 1$ below the threshold. The annihilation of the pumping photon provides energy to cavity C_2 and generates a low-frequency signal photon and an idle photon. As a result, the number of signal photons increases, which leads to an optical amplification effect.

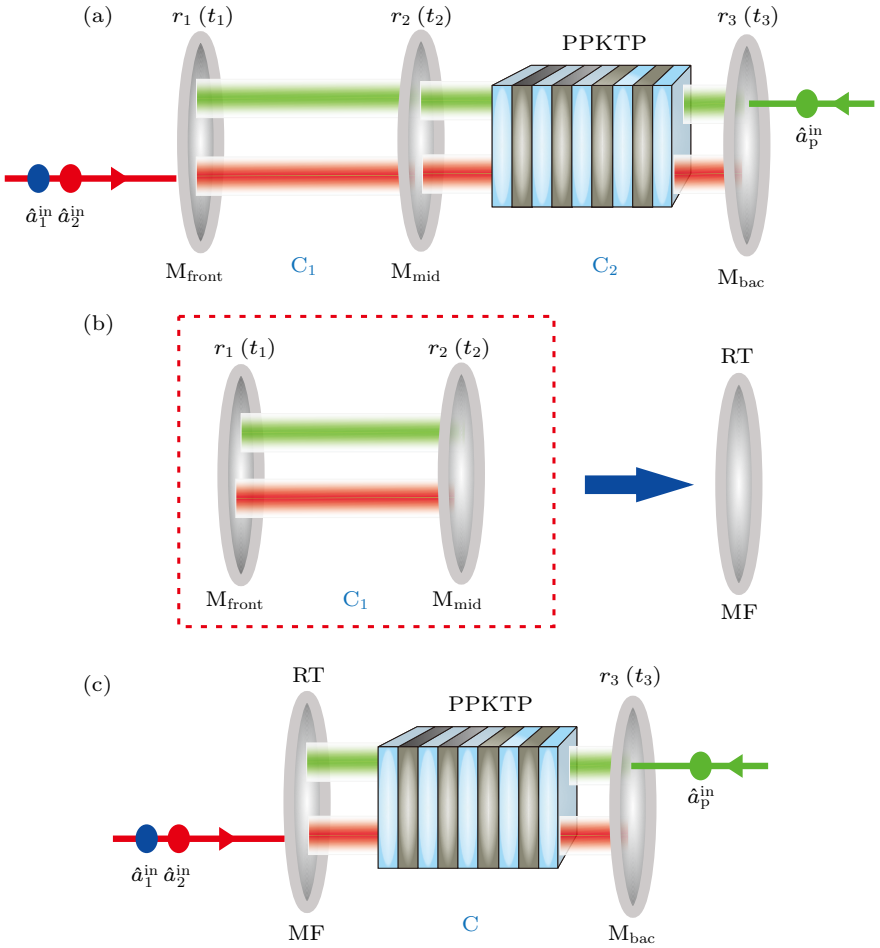


Fig. 1. Scheme diagram of coupling resonant system. (a) The coupling resonant cavity model. Optical cavity C_1 and optical cavity C_2 are coupling by a middle mirror M_{mid}; $r_1(t_1)$, $r_2(t_2)$ and $r_3(t_3)$ denote the reflection (transmission) coefficients for cavity mirrors M_{front}, M_{mid}, and M_{bac}, respectively. Signal light a_1^{in} and idle light a_2^{in} are light fields with entanglement properties. (b) An equivalent model diagram based on the input-output relationship and the strength of the optical field at different positions in the optical cavity C_1. $R(T)$ is the total reflectance (transmittance) of cavity C_1. (c) The diagram of simplified coupling resonant system model.

We adopt a semi-classical approach to superimpose cavity C_1 as shown in Fig. 1(b).[23,24] The reflection coefficient of the whole cavity C_1 can be obtained from the relationship between the input and output of the light field in a single optical cavity. The cavity C_1 is physically equivalent to the front cavity mirror MF, which eventually enables the coupled resonant cavity model to be simplified to a single cavity system as shown in Fig. 1(c). The coupling strength of the two cavities (C_1 and C_2) can be effectively controlled by adjusting the transmission coefficient of the intermediate cavity mirror

M_{mid}. Therefore, the superimposed system model (Fig. 1(c)) also has the characteristics of a coupled resonant cavity. The Hamiltonian of the system (Fig. 1(c)) can be written as[25–27]

$$\begin{aligned} H =& \hbar\omega_{\rm p}\hat{a}_{\rm p}^{+}\hat{a}_{\rm p}+\hbar\omega_1\hat{a}_1^{+}\hat{a}_1+\hbar\omega_2\hat{a}_2^{+}\hat{a}_2 \\ &+{\rm i}\hbar K(\hat{a}_1^{+}\hat{a}_2^{+}\hat{a}_{\rm p}-\hat{a}_1\hat{a}_2\hat{a}_{\rm p}^{+})+{\rm i}\hbar(E_{\rm p}\hat{a}_{\rm p}^{+}{\rm e}^{-{\rm i}\omega_{\rm p}t} \\ &+E_1\hat{a}_1^{+}{\rm e}^{-{\rm i}\omega_1 t}+E_2\hat{a}_2^{+}{\rm e}^{-{\rm i}\omega_2 t}+{\rm H.c.}), \end{aligned} \tag{1}$$

where the first three terms represent the free Hamiltonian of the pumping light, signal field and idle field, respectively; $\hat{a}_j$ ($\hat{a}_j^{+}$) ($[\hat{O}_j,\hat{O}_j^{+}]=1$, $\hat{O}_j=\hat{a}_j$, $j={\rm p},1,2$) are the annihilation (creation) operator of the pumping, signal and idle modes, respectively; $\omega_{\rm p}$, ω_1 and ω_2 are frequencies of the pumping, signal and idle modes. The fourth term denotes interaction of different modes. K is effective second-order nonlinearity of the crystal.[25] The last item denotes the laser input driving with frequency ω_0^j. $E_j=\sqrt{2P_j\gamma_j/\hbar\omega_0^j}$ describes the coupling strength of the optical cavity and each light field. P_j is the power of light field with frequency ω_0^j, and $\gamma_j=\gamma_f^j+\gamma_{\rm out}^j$ is the total decay rate of the pump and signal modes in the cavity; γ_f^j ($\gamma_{\rm out}^j$) denotes the decay rate of $\hat{a}_j$ through the front and middle (back) cavity mirrors.

The coupling resonant cavity system model can produce multi-channel quantum interference effects compared to single cavity (without middle mirror M_{mid}). The reflection coefficient R of the overall cavity C_1 can be obtained according to the input–output relationship and the strength of the optical field at different positions[24]

$$R=\frac{r_2-\gamma_{\rm c}r_1\exp(2{\rm i}\omega_j L/c)}{1-\gamma_{\rm c}r_1r_2\exp(2{\rm i}\omega_j L/c)}, \tag{2}$$

where L is the length of cavity C_1, ω_j is the optical field frequency, $\gamma_{\rm c}$ represents other decay effects in cavity C_1.

The Langevin equation for different modes can be obtained by the equation $\dot{\hat{O}}_j=(1/{\rm i}\hbar)[\hat{O}_j,H_0]-\gamma_j\hat{O}_j+\hat{O}_j^{\rm in}$.[28] Consider the dissipation and input noise of each mode, the Langevin equations of motion for our system can be written as[29,30]

$$\begin{aligned} \dot{\hat{a}}_1 =& (-{\rm i}\Delta_1-\gamma_1)\hat{a}_1+K\hat{a}_{\rm p}\hat{a}_2^{+}+E_1 \\ &+\sqrt{2\gamma_1^{\rm in}}\hat{a}_1^{\rm in}+\sqrt{2\gamma_1^{\rm out}}\hat{a}_1^{\rm v}, \end{aligned} \tag{3a}$$

$$\begin{aligned} \dot{\hat{a}}_2 =& (-{\rm i}\Delta_2-\gamma_2)\hat{a}_2+K\hat{a}_{\rm p}\hat{a}_1^{+}+E_2 \\ &+\sqrt{2\gamma_2^{\rm in}}\hat{a}_2^{\rm in}+\sqrt{2\gamma_2^{\rm out}}\hat{a}_2^{\rm v}, \end{aligned} \tag{3b}$$

$$\begin{aligned} \dot{\hat{a}}_{\rm p} =& (-{\rm i}\Delta_{\rm p}-\gamma_{\rm p})\hat{a}_{\rm p}+K\hat{a}_1\hat{a}_2^{+}+E_{\rm p} \\ &+\sqrt{2\gamma_{\rm p}^{\rm in}}\hat{a}_{\rm p}^{\rm in}+\sqrt{2\gamma_{\rm p}^{\rm out}}\hat{a}_{\rm p}^{\rm v}, \end{aligned} \tag{3c}$$

where $\Delta_j=\omega_j-\omega_0^j$ ($j=1,2,{\rm p}$); $\gamma_j^{\rm in}=\gamma_f^j+\gamma_{\rm c}=\sqrt{1-R^2}$ describes the decay rate of optical field $\hat{a}_j$ going through front cavity mirror M_{front} and middle cavity mirror M_{mid} (cavity C_1) and other decay effects in cavity C_1.[24] We define pumping light $\hat{a}_{\rm p}=\beta\exp({\rm i}\theta)$. Here β (θ) is the amplitude (phase) of the pumping light. The noise correlation function of the input optical field $a_j^{\rm in}$ and the vacuum field $\hat{a}_j^{\rm v}$ can be expressed as[31]

$$\begin{aligned} &\langle Q(t)Q^{+}(t')\rangle=[N+1]\delta(t-t'), \\ &\langle Q^{+}(t)Q(t')\rangle=N\delta(t-t'), \\ &\langle Q(t)Q(t')\rangle=M\exp[-{\rm i}\Delta_j(t+t')]\delta(t-t'), \\ &\langle Q^{+}(t)Q^{+}(t')\rangle=M^{*}\exp[{\rm i}\Delta_j(t+t')]\delta(t-t'), \\ &Q(t)=\hat{a}_j^{\rm in},\ \hat{a}_j^{\rm v},\quad N=\sinh^2 s, \\ &M=\exp({\rm i}\theta_{\rm c})\sinh s\cosh s, \end{aligned}$$

where $\theta_{\rm c}$ denotes the phase between the quantum correlation signal field and the idle field, and s is the squeezing parameter of squeezed field. The squeezing parameter $s=0$ when $Q(t)=\hat{a}_j^{\rm v}$.

The operator can be expressed as a steady-state value plus a small quantum fluctuation term, i.e., $\hat{a}_j=\bar{a}_j+\delta\hat{a}_j$. The quadrature operators are defined as $\delta\hat{X}=(\delta\hat{a}+\delta\hat{a}^{+})/\sqrt{2}$, $\delta\hat{Y}={\rm i}(\delta\hat{a}^{+}-\delta\hat{a})/\sqrt{2}$.[32] Thus, the quantum noise quadrature component of the output can be expressed as[17]

$$\begin{aligned} \delta\hat{X}_{\rm c} &= \frac{1}{\sqrt{2}}(\delta\hat{a}_1+\delta\hat{a}_2+\delta\hat{a}_1^{+}+\delta\hat{a}_2^{+}) \\ &= \frac{1}{\sqrt{2}}(\delta\hat{X}_{a1}+\delta\hat{X}_{a2}), \end{aligned} \tag{4a}$$

$$\begin{aligned} \delta\hat{Y}_{\rm c} &= \frac{1}{\sqrt{2}i}(\delta\hat{a}_1+\delta\hat{a}_2-\delta\hat{a}_1^{+}-\delta\hat{a}_2^{+}) \\ &= \frac{1}{\sqrt{2}}(\delta\hat{Y}_{a1}+\delta\hat{Y}_{a2}), \end{aligned} \tag{4b}$$

$$\begin{aligned} \delta\hat{X}_{\rm d} &= \frac{1}{\sqrt{2}}(\delta\hat{a}_1-\delta\hat{a}_2+\delta\hat{a}_1^{+}-\delta\hat{a}_2^{+}) \\ &= \frac{1}{\sqrt{2}}(\delta\hat{X}_{a1}-\delta\hat{X}_{a2}), \end{aligned} \tag{4c}$$

$$\begin{aligned} \delta\hat{Y}_{\rm d} &= \frac{1}{\sqrt{2}i}(\delta\hat{a}_1-\delta\hat{a}_2-\delta\hat{a}_1^{+}+\delta\hat{a}_2^{+}) \\ &= \frac{1}{\sqrt{2}}(\delta\hat{Y}_{a1}-\delta\hat{Y}_{a2}). \end{aligned} \tag{4d}$$

By linearizing Eq. (3), we take the Langevin equations of motion into the Eq. (4) and make the Fourier transform read

$$\begin{aligned} -{\rm i}\omega\delta\hat{X}_{\rm c}(\omega) =& \Delta_1\delta\hat{Y}_{\rm c}(\omega)-\gamma_1\delta\hat{X}_{\rm c}(\omega)+K\delta\hat{X}_{\rm c}^{\theta}(\omega) \\ &+\sqrt{2\gamma_1^{\rm in}}\delta\hat{X}_{\rm c}^{\rm in}+\sqrt{2\gamma_1^{\rm out}}\delta\hat{X}_{\rm c}^{\rm v}, \end{aligned} \tag{5a}$$

$$\begin{aligned} -{\rm i}\omega\delta\hat{Y}_{\rm c}(\omega) =& -\Delta_1\delta\hat{X}_{\rm c}(\omega)-\gamma_1\delta\hat{Y}_{\rm c}(\omega)-K\delta\hat{Y}_{\rm c}^{\theta}(\omega) \\ &+\sqrt{2\gamma_1^{\rm in}}\delta\hat{Y}_{\rm c}^{\rm in}+\sqrt{2\gamma_1^{\rm out}}\delta\hat{Y}_{\rm c}^{\rm v}, \end{aligned} \tag{5b}$$

$$\begin{aligned} -{\rm i}\omega\delta\hat{X}_{\rm d}(\omega) =& \Delta_2\delta\hat{Y}_{\rm d}(\omega)-\gamma_2\delta\hat{X}_{\rm d}(\omega)-K\delta\hat{X}_{\rm d}^{\theta}(\omega) \\ &+\sqrt{2\gamma_2^{\rm in}}\delta\hat{X}_{\rm d}^{\rm in}+\sqrt{2\gamma_2^{\rm out}}\delta\hat{X}_{\rm d}^{\rm v}, \end{aligned} \tag{5c}$$

$$\begin{aligned} -{\rm i}\omega\delta\hat{Y}_{\rm d}(\omega) =& -\Delta_2\delta\hat{X}_{\rm d}(\omega)-\gamma_2\delta\hat{Y}_{\rm d}(\omega)+K\delta\hat{Y}_{\rm d}^{\theta}(\omega) \\ &+\sqrt{2\gamma_2^{\rm in}}\delta\hat{Y}_{\rm d}^{\rm in}+\sqrt{2\gamma_2^{\rm out}}\delta\hat{Y}_{\rm d}^{\rm v}, \end{aligned} \tag{5d}$$

where

$$\delta\hat{X}_{\rm c}^{\theta}(\omega)=\frac{1}{\sqrt{2}}(\delta\hat{a}_1{\rm e}^{-{\rm i}\theta}+\delta\hat{a}_2{\rm e}^{-{\rm i}\theta}+\delta\hat{a}_1^{+}{\rm e}^{{\rm i}\theta}+\delta\hat{a}_2^{+}{\rm e}^{{\rm i}\theta}), \quad (6a)$$

$$\delta\hat{Y}_{\rm c}^{\theta}(\omega)=\frac{1}{{\rm i}\sqrt{2}}(\delta\hat{a}_1{\rm e}^{-{\rm i}\theta}+\delta\hat{a}_2{\rm e}^{-{\rm i}\theta}-\delta\hat{a}_1^{+}{\rm e}^{{\rm i}\theta}-\delta\hat{a}_2^{+}{\rm e}^{{\rm i}\theta}), \quad (6b)$$

$$\delta\hat{X}_{\rm d}^{\theta}(\omega)=\frac{1}{\sqrt{2}}(\delta\hat{a}_1{\rm e}^{-{\rm i}\theta}-\delta\hat{a}_2{\rm e}^{-{\rm i}\theta}+\delta\hat{a}_1^{+}{\rm e}^{{\rm i}\theta}-\delta\hat{a}_2^{+}{\rm e}^{{\rm i}\theta}), \quad (6c)$$

$$\delta\hat{Y}_{\rm d}^{\theta}(\omega)=\frac{1}{{\rm i}\sqrt{2}}(\delta\hat{a}_1{\rm e}^{-{\rm i}\theta}-\delta\hat{a}_2{\rm e}^{-{\rm i}\theta}-\delta\hat{a}_1^{+}{\rm e}^{{\rm i}\theta}+\delta\hat{a}_2^{+}{\rm e}^{{\rm i}\theta}). \quad (6d)$$

According to the input-output theory we have $\delta\hat{X}_i^{\rm o}=-\delta\hat{X}_i^{\rm in}+\sqrt{2\gamma_j^{\rm in}}\delta\hat{X}_i$ ($i={\rm c},\ {\rm d}$). Since the signal light and the idle light have the same frequency $\omega_1=\omega_2=\omega$, we assume that the decay rate (detuning) of the signal light and the idle light are equal to each other, i.e., $\gamma_1=\gamma_2=\gamma$, $\gamma_1^k=\gamma_1^k=\gamma^k$ ($k={\rm in},\ {\rm out}$), $\Delta_1=\Delta_2=\Delta$. The quantum correlation spectrum quadrature amplitude for the output signal and the idle mode in terms of input fluctuations can be obtained as follows:[17,33]

$$\begin{aligned}\delta\hat{X}_i^{\rm o}(\omega)=&\big[P'_{\hat{X}_{\rm c}^{\rm o}}\delta\hat{X}_i^{\rm in}(\omega)+Q'_{\hat{X}_{\rm c}^{\rm o}}\delta\hat{Y}_i^{\rm in}(\omega)+M'_{\hat{X}_{\rm c}^{\rm o}}\delta\hat{X}_i^{\rm v}(\omega)\\&+N'_{\hat{X}_{\rm c}^{\rm o}}\delta\hat{Y}_i^{\rm v}(\omega)\big]\cdot\big[\gamma^2+(\Delta\tau)^2-(\tau\omega)^2-(K\beta)^2\\&+2\tau{\rm i}\omega\gamma\big]^{-1}. \quad (7)\end{aligned}$$

Similarly, the quantum correlation spectrum of quadrature phase is obtained as

$$\begin{aligned}\delta\hat{Y}_i^{\rm o}(\omega)=&\big[P'_{\hat{Y}_i^{\rm o}}\delta\hat{Y}_i^{\rm in}(\omega)+Q'_{\hat{Y}_i^{\rm o}}\delta\hat{X}_i^{\rm in}(\omega)+M'_{\hat{Y}_i^{\rm o}}\delta\hat{Y}_i^{\rm v}(\omega)\\&+N'_{\hat{Y}_i^{\rm o}}\delta\hat{X}_i^{\rm v}(\omega)\big]\cdot\big[\gamma^2+(\Delta\tau)^2-(\tau\omega)^2-(K\beta)^2\\&+2\tau{\rm i}\omega\gamma\big]^{-1}. \quad (8)\end{aligned}$$

Here, the parameters $P'_{\hat{X}_{\rm c}^{\rm o}}$, $Q'_{\hat{X}_{\rm c}^{\rm o}}$, $M'_{\hat{X}_{\rm c}^{\rm o}}$, $N'_{\hat{X}_{\rm c}^{\rm o}}$ are given as follows:

$$\begin{aligned}P'_{\hat{X}_{\rm c}^{\rm o}}=&\gamma^2+(\tau\omega)^2-(\Delta\tau)^2+(K\beta)^2\pm2K\beta\gamma^{\rm in}\cos\theta\\&+2{\rm i}\tau\omega(\gamma-\gamma^{\rm in}), \quad (9a)\end{aligned}$$

$$Q'_{\hat{X}_{\rm c}^{\rm o}}=2\gamma(\Delta\tau\pm K\beta\sin\theta), \quad (9b)$$

$$M'_{\hat{X}_{\rm c}^{\rm o}}=2\sqrt{\gamma^{\rm in}\gamma^{\rm out}}(\gamma\pm K\beta\cos\theta+{\rm i}\tau\omega), \quad (9c)$$

$$N'_{\hat{X}_{\rm c}^{\rm o}}=2\sqrt{\gamma^{\rm in}\gamma^{\rm out}}(\Delta\tau\pm K\beta\sin\theta). \quad (9d)$$

Equations (9a)–(9d) get plus signs when $i={\rm c}$, and they get minus signs when $i={\rm d}$. The parameters $P'_{\hat{Y}_i^{\rm o}}$, $Q'_{\hat{Y}_i^{\rm o}}$, $M'_{\hat{Y}_i^{\rm o}}$, $N'_{\hat{Y}_i^{\rm o}}$ are given by

$$\begin{aligned}P'_{\hat{Y}_i^{\rm o}}=&\gamma^2+(\tau\omega)^2-(\Delta\tau)^2+(K\beta)^2+2K\beta\gamma^{\rm in}\cos\theta\\&+2{\rm i}\tau\omega(\gamma-\gamma^{\rm in}), \quad (10a)\end{aligned}$$

$$Q'_{\hat{Y}_i^{\rm o}}=2\gamma(\Delta\tau\mp K\beta\sin\theta), \quad (10b)$$

$$M'_{\hat{Y}_i^{\rm o}}=2\sqrt{\gamma^{\rm in}\gamma^{\rm out}}(\gamma\mp K\beta\cos\theta+{\rm i}\tau\omega), \quad (10c)$$

$$N'_{\hat{Y}_i^{\rm o}}=2\sqrt{\gamma^{\rm in}\gamma^{\rm out}}(\Delta\tau\mp K\beta\sin\theta). \quad (10d)$$

Equations (10a)–(10d) get plus signs when $i={\rm d}$, and they get minus signs when $i={\rm c}$.

Subsequently, the final quantum noise correlated variance fluctuation equation of quadrature amplitude for signal light and idle frequency light is obtained as follows:[15,33]

$$\begin{aligned}\delta^2\hat{X}_i^{\rm o}(\omega)=&\big\{P_{\hat{X}_i^{\rm o}}\delta^2\hat{X}_i^{\rm in}(\omega)+Q_{\hat{X}_i^{\rm o}}\delta^2\hat{Y}_i^{\rm in}(\omega)+M_{\hat{X}_i^{\rm o}}\delta^2\hat{X}_i^{\rm v}(\omega)\\&+N_{\hat{X}_i^{\rm o}}\delta^2\hat{Y}_i^{\rm v}(\omega)\big\}\cdot\big\{[\gamma^2+(\Delta\tau)^2-(\tau\omega)^2\\&-(K\beta)^2]^2+4(\tau\omega\gamma)^2\big\}^{-1}. \quad (11)\end{aligned}$$

Similarly, the noise covariance of quadrature phase is obtained to be

$$\begin{aligned}\delta^2\hat{Y}_i^{\rm o}(\omega)=&\big\{P_{\hat{Y}_i^{\rm o}}\delta^2\hat{Y}_i^{\rm in}(\omega)+Q_{\hat{Y}_i^{\rm o}}\delta^2\hat{X}_i^{\rm in}(\omega)+M_{\hat{Y}_i^{\rm o}}\delta^2\hat{Y}_i^{\rm v}(\omega)\\&+N_{\hat{Y}_i^{\rm o}}\delta^2\hat{X}_i^{\rm v}(\omega)\big\}\cdot\big\{[\gamma^2+(\Delta\tau)^2-(\tau\omega)^2\\&-(K\beta)^2]^2+4(\tau\omega\gamma)^2\big\}^{-1}. \quad (12)\end{aligned}$$

Here, the parameters $P_{\hat{X}_i^{\rm o}}$, $Q_{\hat{X}_i^{\rm o}}$, $M_{\hat{X}_i^{\rm o}}$, $N_{\hat{X}_i^{\rm o}}$ are given as

$$\begin{aligned}P_{\hat{X}_i^{\rm o}}=&[\gamma^2+(\tau\omega)^2-(\Delta\tau)^2+(K\beta)^2\pm2K\beta\gamma^{\rm in}\cos\theta]^2\\&+4(\tau\omega)^2(\gamma-\gamma^{\rm in})^2, \quad (13a)\end{aligned}$$

$$Q_{\hat{X}_i^{\rm o}}=4\gamma^2(\Delta\tau\pm K\beta\sin\theta)^2, \quad (13b)$$

$$M_{\hat{X}_i^{\rm o}}=4\gamma^{\rm in}\gamma^{\rm out}[(\gamma\pm K\beta\cos\theta)^2+(\tau\omega)^2], \quad (13c)$$

$$N_{\hat{X}_i^{\rm o}}=4\gamma^{\rm in}\gamma^{\rm out}(\Delta\tau\pm K\beta\sin\theta)^2. \quad (13d)$$

Equations (13a)–(13d) get plus signs when $i={\rm c}$, and they get minus signs when $i={\rm d}$. The parameters $P_{\hat{Y}_i^{\rm o}}$, $Q_{\hat{Y}_i^{\rm o}}$, $M_{\hat{Y}_i^{\rm o}}$, $N_{\hat{Y}_i^{\rm o}}$ are given as

$$\begin{aligned}P_{\hat{Y}_{\rm c}^{\rm o}}=&[\gamma^2+(\tau\omega)^2-(\Delta\tau)^2+(K\beta)^2\mp2K\beta\gamma^{\rm in}\cos\theta]^2\\&+4(\tau\omega)^2(\gamma-\gamma^{\rm in})^2, \quad (14a)\end{aligned}$$

$$Q_{\hat{Y}_{\rm c}^{\rm o}}=4\gamma^2(\Delta\tau\mp K\beta\sin\theta)^2, \quad (14b)$$

$$M_{\hat{Y}_{\rm c}^{\rm o}}=4\gamma^{\rm in}\gamma^{\rm out}[(\gamma\mp K\beta\cos\theta)^2+(\tau\omega)^2], \quad (14c)$$

$$N_{\hat{Y}_{\rm c}^{\rm o}}=4\gamma^{\rm in}\gamma^{\rm out}(\Delta\tau\mp K\beta\sin\theta)^2. \quad (14d)$$

Equations (14a)–(14d) get plus signs when $i={\rm d}$, and they get minus signs when $i={\rm c}$. In the above equations, $\delta^2\hat{X}_{\rm c}^{\rm in}(\omega)=\delta^2\hat{X}_{\rm d}^{\rm in}(\omega)={\rm e}^{2s}$, $\delta^2\hat{Y}_{\rm c}^{\rm in}(\omega)=\delta^2\hat{Y}_{\rm d}^{\rm in}(\omega)={\rm e}^{-2s}$, where s is the squeezing parameter. Since vacuum input, $\delta^2\hat{X}_{\rm c}^{\rm v}(\omega)=\delta^2\hat{Y}_{\rm c}^{\rm v}(\omega)=\delta^2\hat{X}_{\rm d}^{\rm v}(\omega)=\delta^2\hat{Y}_{\rm d}^{\rm v}(\omega)=1$.

As shown in the following equation, Duan and Simon proposed a non-separability criterion for two-mode measurable squeeze variance.[34,35] Specifically, a sufficient condition for entanglement is that the correlated quadrature components satisfy the inequality

$$\delta^2\langle\hat{X}_1^{\rm o}\pm\hat{X}_2^{\rm o}\rangle+\delta^2\langle\hat{Y}_1^{\rm o}\mp\hat{Y}_2^{\rm o}\rangle<4. \quad (15)$$

3. Discussion

3.1. A weak coupling resonant cavity with entangled state

Figure 2 shows multi-channel quantum interference phenomenon and quantum entanglement results with the pumping power $E_{\rm th}=0.2\beta_{\rm th}$ ($E_{\rm th}=0.5\beta_{\rm th}$).

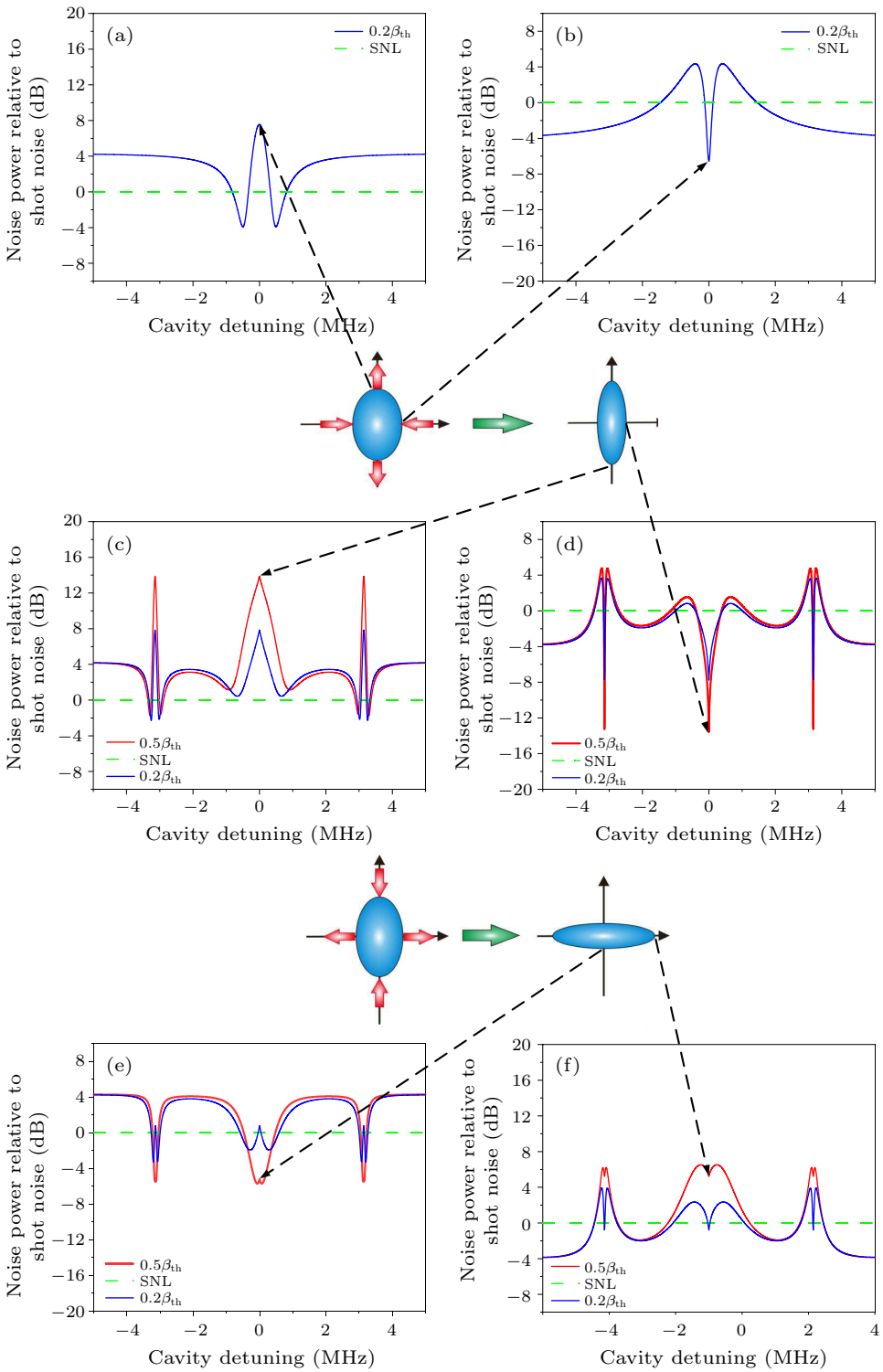


Fig. 2. Quantum covariance function in weak coupling resonant cavity. The green curves denote the shot-noise limit (SNL). The intensity of the pumping power at $0.2\beta_{th}$ ($0.5\beta_{th}$) is blue (red). [(a), (b)] The quadrature amplitude (a) and quadrature phase distribution function (b) of the entangled beam pair in a single cavity. [(c), (d)] Quadrature amplitude $\hat{X}_c$ (c) and phase $\hat{Y}_c$ (d) when the pumping light phase is $\theta = 0$. [(e), (f)] Quadrature amplitude $\hat{X}_d$ (e) and phase $\hat{Y}_d$ (f) when the pumping light phase is $\theta = \pi$.

Firstly, we focus on the single cavity model which can be achieved by removing the cavity mirror M_{mid} of the coupling resonant system. The transmission parameters of the front mirror and back mirror are $t_1 = 0.0016$ and $t_3 = 0.00005$.[17,36] A continuous variable entangled beam injects into the single cavity, and the quantum noise correlation curves are shown in Figs. 2(a) and 2(b). Figure 2(a) provides a curve of quantum noise fluctuations at quadrature amplitude. Due to the non-degenerate OPA, the signal field and idle field interactions at the $\Delta = 0$ MHz, the curve is amplified and two weak squeezed states appear at two sidebands. The overall curve shows an EIT-like line shape. Figure 2(b) shows the quantum fluctuation noise curve at the quadrature phase. Due to the Heisenberg uncertainty principle, the quantum noise fluctuation curve at the

quadrature phase shows a squeezed state. The degree of noise suppression is up to 6.55 dB at the quadrature phase.

Next, we consider the weak coupling resonant system with three mirrors M_{front}, M_{mid} and M_{bac}. Coupling strength of cavities C_1 and C_2 depends on the transmittance of the middle mirror M_{mid}. According to the accessible parameters in experiments by Di *et al.*,[18] the parameters of the mirrors in the coupling resonant cavity are adjusted as follows: $t_1 = 0.05$, $t_2 = 0.014$, $t_3 = 0.002$. In the coupling resonant system, the quantum interference effect is significantly enhanced compared to the single cavity system. The quantum noise fluctuation curves of the pumping phase at $\theta = 0$ are shown in Figs. 2(c) and 2(d). Due to the coupling of cavities C_1 and C_2, multi-channel quantum interference phenomena can be observed from Figs. 2(c) and 2(d). They are simultaneously distributed at different detuning frequencies $\Delta = 0$ MHz and $\Delta = \pm 3.1$ MHz, respectively. These EIT-like multi-channel quantum interference effects are more sensitive to pumping light. Strong pumping power can effectively enhance the quantum interference phenomenon in each channel. Meanwhile, we adjust the phase θ from 0 to π of the pumping light to achieve phase-sensitive modulation. As shown in Fig. 2(e), the peaks at different detuning frequencies switch from positive to negative values. In contrast, the peaks at different detuning frequencies switch from negative value to positive value in Fig. 2(f). Phase-sensitive modulation achieves multi-channel quantum noise suppression of quadrature amplitude while sacrificing bandwidth compared to Figs. 2(c) and 2(d). However, the bandwidth of the EIT-like quantum interference channel at the $\Delta = 0$ MHz detuning is obviously broadened in comparison to the single cavity system.

3.2. A strong coupling resonant cavity with entangled state

Figure 3 shows the quantum interference properties of the entangled light in the strong coupling resonant system. The coupling strength depends on the transmittance t_2 of the middle mirror M_{mid}. We change the transmittance $t_2 = 0.15$ of the middle mirror M_{mid} and the other parameters are the same as those of the weak coupling resonant cavity. Owing to the increasing coupling strength between cavities C_1 and C_2, all the quantum interference channels are effectively broadened, compared to weak coupling resonator system.

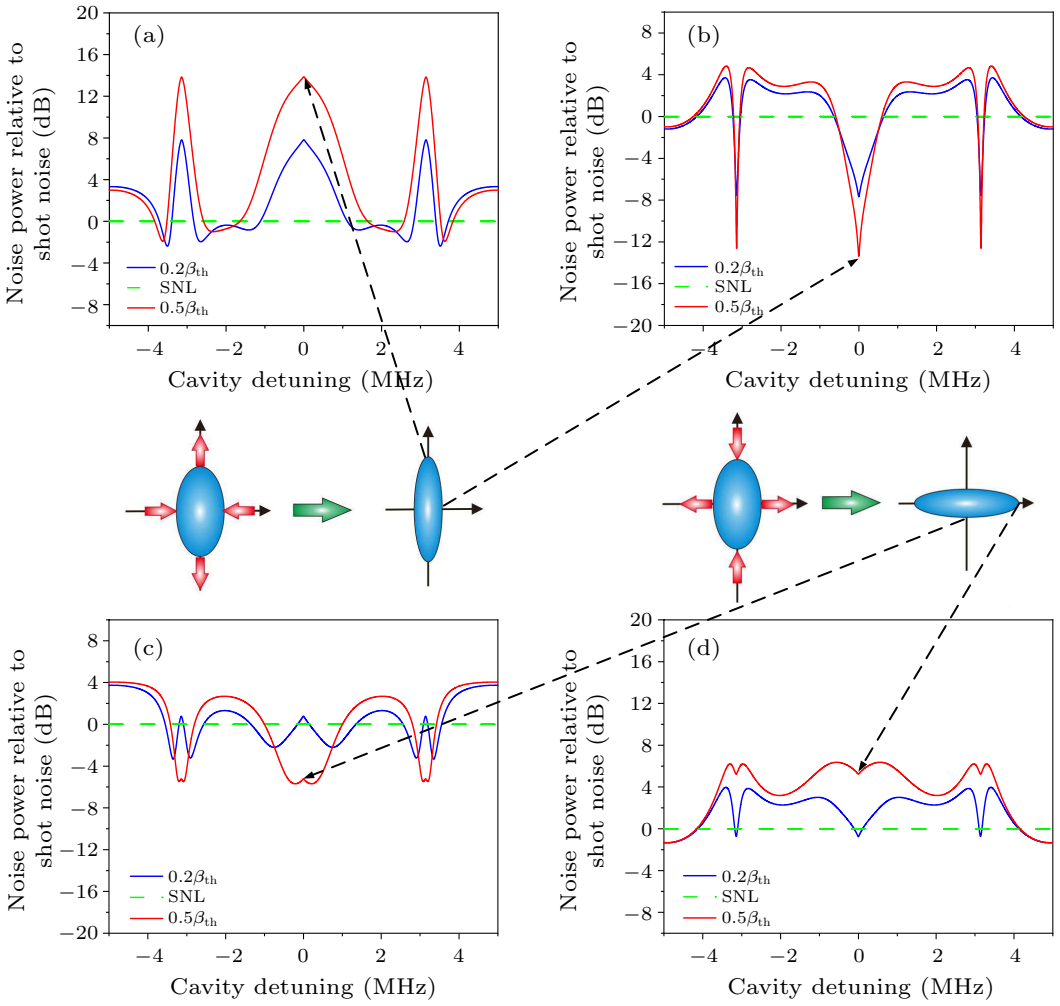


Fig. 3. Quantum covariance function in strong coupling resonant cavity. [(a), (b)] Quadrature amplitude $\hat{X}_c$ and phase $\hat{Y}_c$ with $\theta = 0$. [(c), (d)] Quadrature amplitude $\hat{X}_d$ and phase $\hat{Y}_d$ with $\theta = \pi$. The transmittance of the middle mirror M_{mid} is $t_2 = 0.15$. Other parameters are the same as those of the weak coupling resonant system.

Quantum interference channel is broadened 2.17 times at the $\Delta = 0$ MHz compared to single cavity resonant cavity. Meanwhile, the quantum interference channel of the strong coupling resonant cavity at the $\Delta = 0$ MHz ($\Delta = \pm 3.1$ MHz) is broadened up to 1.27 (3.53) times compared to that of the weak coupling resonant system. In addition, it can also be achieved to broaden the EIT-like quantum interference windows by appropriately increasing the pumping optical power. Wider EIT-like window can be better matched to the detection pulse and a larger group delay can be obtained.[37] The generation of multiple broadband EIT-like quantum interference channels facilitates improving the efficiency of wave packet propagation and reducing the distortion rate during acquisition of quantum information.[38–40]

3.3. Analysis of entanglement properties in different systems

Figure 4 show the entanglement properties of the single cavity and coupling resonant system. From Fig. 4(a), we observe that the entanglement strength of the output field is highest at $\Delta = 0$ MHz and two weak entangled state appear symmetrically on both sides of the $\Delta = 0$ MHz.

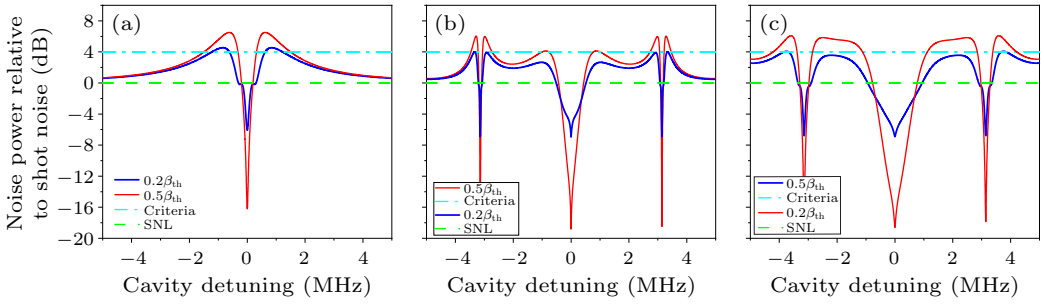


Fig. 4. The entanglement results of (a) signal light and idle light in single cavity, (b) weak coupling resonant system, and (c) strong coupling resonant system. The cyan curves denote non-separability criterion. Other parameters are the same as those of the weak coupling resonant system.

In Fig. 4(b), it can be clearly seen that entanglement exists at the central frequencies of EIT-like multiple quantum interference channels. The entanglement strength is up to 19.8 dB when the pumping light power is $0.5\beta_{th}$. A strong coupling resonant system can be realized when $t_2 = 0.15$. The entanglement properties of each quantum interference channel in the strong coupling resonant system are shown in Fig. 4(c). A strong coupling resonant cavity does not enhance the entanglement strength compared to Fig. 4(b). However, the strong coupling resonance system can effectively broaden the quantum interference channel, the range of entanglement is also broadened. The phenomenon of multiple EIT-like quantum interference entanglement channels appearing simultaneously is beneficial to improve the efficiency of quantum information transfer. It has potential applications in the fields of quantum communication[41–43] and quantum storage,[44] etc.

4. Conclusion

In summary, multi-channel quantum noise suppression, phase-sensitive modulation and entanglement properties generated by entangled light are systematically analyzed in a coupling resonant system with different coupling strengths. Compared to the single cavity (weak coupling resonant cavity) system, the bandwidth is broadened by 2.17 (3.53) times with $\Delta = 0$ MHz ($\Delta = \pm 3.1$ MHz) in a strong coupling resonant system. The output field presents entanglement properties at multiple frequencies, which can effectively enhance the information carrying capacity of quantum communication systems. Our results have potential applications in fields of quantum information processing,[40,45] multi-channel EIT memory,[46] and quantum precision measurement,[47–49] etc.

Acknowledgments

Project supported by National Natural Science Foundation of China (Grant Nos. 11704053 and 52175531) and the Science and Technology Research Program of Chongqing Municipal Education Commission (Grant No. KJQN201800629).

References

[1] Owens I J, Hughes R J and Nordholt J E 2008 *Phys. Rev. A* **78** 022307
[2] Pivoluska M, Huber M and Malik M 2018 *Phys. Rev. A* **97** 032312
[3] Kogias I, Xiang Y, He Q and Adesso G 2017 *Phys. Rev. A* **95** 012315
[4] Williams B P, Lukens J M, Peters N A, Qi B and Grice W P 2019 *Phys. Rev. A* **99** 062311
[5] Barasiński A, Černoch A and Lemr K 2019 *Phys. Rev. Lett.* **122** 170501
[6] Yang L, Liu Y C and Li Y S 2020 *Chin. Phys. B* **29** 60301
[7] Mukamel Gu B and Manipulating S 2020 *J. Phys. Chem. Lett.* **11** 8177
[8] Qiu T H, Li H, Xie M, Liu Q and Ma H Y 2019 *Opt. Express* **27** 27477
[9] Braunstein S and Loock P 2005 *Rev. Mod. Phys.* **77** 513
[10] Chen Z B, Lu C Y, Weinfurter H, Zeilinger A and Żukowsk M 2012 *Rev. Mod. Phys.* **84** 777
[11] Feng J X, Wan Z J, Li Y J and Zhang K S 2018 *Laser Phys. Lett.* **15** 015209
[12] Wen F, Hui S J, Zhang S W, Wu Z K, Liu Z C, Zhu T F, Lin F, Wang W, Zhang Y P and Wang H X 2022 *Ann. Phys.* **534** 2100396
[13] Lenzini F, Janousek J, Thearle O, Villa M, Haylock B and Kasture S 2018 *Sci. Adv.* **4** eaat9331
[14] Dias J, Hosseinidehaj N and Ralph T C 2020 *Phys. Rev. A* **102** 052425
[15] Ma H L, Ye C G, Wei D and Zhang J 2005 *Phys. Rev. Lett.* **95** 233601
[16] Agarwal G S 2006 *Phys. Rev. Lett.* **97** 023601
[17] Chen H X and Zhang J 2009 *Phys. Rev. A* **79** 063826
[18] Di K, Xie C D and Zhang J 2011 *Phys. Rev. Lett.* **106** 153602
[19] Jia X, Yan Z, Liang W, Liu Y and Peng K 2017 *Nat. Commun.* **8** 718
[20] Wei X, Wang Y, Zhang J and Zhu Y 2011 *Phys. Rev. A* **84** 045806

[21] Huang G and Shou C 2020 *Opt. Lett.* **45** 6787
[22] Wei, Y C, Wu B H, Hsiao Y F, Tsai P J and Chen Y C 2020 *Phys. Rev. A* **102** 063720
[23] Smith D D and Chang H 2004 *J. Mod. Opt.* **51** 2503
[24] Smith D D, Chang H, Fuller K A, Rosenberger A T and Boyd R W 2004 *Phys. Rev. A* **69** 063804
[25] Lane A S, Reid M D and Walls D F 1988 *Phys. Rev. A* **38** 788
[26] Ou Z Y, Pereira S F, Kimble H J and Peng K C 1992 *Phys. Rev. Lett.* **68** 3663
[27] Harrison F E and Walls D F 1995 *Opt. Commun.* **123** 331
[28] Pan G X, Xiao R J and Zhou L 2016 *Int. J. Theor. Phys.* **55** 3697
[29] Lawrence M J, Byer R L, Fejer M M, Bowen W, Lam P K and Bachor H A 2002 *J. Opt. Soc. Am. B* **19** 1592
[30] Fabre C, Gicobino E and Heidman A 1989 *J. Phys. France* **15** 1209
[31] Aspelmeyer M, Kippenberg T J and Marquardt F 2014 *Rev. Mod. Phys.* **86** 1391
[32] Zhao C Y, Ye X Z, Yang C F and Chen L Y 2012 *Chin. Phys. B* **21** 070308
[33] Zhao C Y and Tan W H 2010 *Chin. Phys. B* **19** 030312
[34] Duan L M, Giedke G, Cirac J I and Zoller P 2000 *Phys. Rev. Lett.* **84** 2722
[35] Simon R 2000 *Phys. Rev. Lett.* **84** 2726
[36] Zhang J, Ye C G, Gao F and Xiao M 2008 *Phys. Rev. Lett.* **101** 233602
[37] Xiao M, Li Y Q, Jin S Z and Gea-Banacloche J 1995 *Phys. Rev. Lett.* **74** 666
[38] Jensen K, Wasilewski W, Krauter H, Fernholz T, Nielsen B M and Serafini A 2011 *Nat. Phys.* **7** 13
[39] Wang Y F, Li J F, Zhang S C, Su K Y, Zhou Y R, Liao K Y, Du S W, Yan H and Zhu S L 2019 *Nat. Photonics* **13** 346
[40] Sarfaraj M N, Sebait M and Mukhopadhyay S 2022 *Optoelectron. Lett.* **18** 673
[41] Liu Y H, Wu L, Yan Z H, Jia X J and Peng K C 2019 *Acta Phys. Sin.* **68** 034202 (in Chinese)
[42] Bashir F 2022 *Optoelectron. Lett.* **18** 519
[43] Coutinho B C, Munro W J, Nemoto K and Omar Y 2022 *Commum. Phys.* **5** 105
[44] Vernaz-Gris P, Huang K, Cao M, Alexandra S S and Julien L 2018 *Nat. Commun.* **9** 363
[45] Magaña-Loaiza O S and Boyd R W 2019 *Rep. Prog. Phys.* **82** 124401
[46] Lei X, Ma L, Yan J, Zhou X, Yan Z and Jia X 2022 *Adv. Phys. X* **7** 2060133
[47] Ren Z H, Li Y, Li Y N and Li W D 2019 *Acta Phys. Sin.* **68** 040601 (in Chinese)
[48] Peniakov G, Su Z E, Beck A, Cogan D, Amar O and Gershoni D 2020 *Phys. Rev. B* **101** 245406
[49] Zhang S X, Liu T H, Cao S, Liu Y T, Geng S B and Lian Y J 2020 *Chin. Phys. B* **29** 50402